Image and Vision Computing 29 (2011) 533–545

Contents lists available at ScienceDirect

Image and Vision Computing

journal homepage: www.elsevier.com/locate/imavis

Shape ultimate attribute opening ☆

Jorge Hernández, Beatriz Marcotegui *

Mines-ParisTech, CMM, Centre de morphologie mathématique, Mathématiques et Systèmes, 35 rue St Honoré 77305-Fontainebleau-Cedex, France

ARTICLE INFO

Article history:
Received 29 September 2010
Received in revised form 8 March 2011
Accepted 17 May 2011

Keywords:
Ultimate opening
Attribute opening
Mathematical morphology
Shape information
Image segmentation
Facade analysis
Scene-text detection
Cell segmentation

ABSTRACT

The ultimate opening (*UO*) is a powerful segmentation operator recently introduced by Beucher [1]. It automatically selects the most contrasted regions of an image. However, in the presence of nested structures (e.g. text in a signboard or windows in a contrasted facade), interesting structures may be masked by the containing region. In this paper we focus on ultimate attribute openings and we propose a method that improves the results by favoring regions with a predefined shape via a similarity function. An efficient implementation using a max-tree representation of the image is proposed. The method is validated in the framework of three applications: facade analysis, scene-text detection and cell segmentation. Experimental results show that the proposed method yields better segmentation results than *UO*.

1. Introduction

Segmentation is a fundamental problem in image analysis to distinguish between objects of interest and "the rest". It creates a partition of the image into disjoint and uniform regions, according to some features such as gray value, color, or texture [2]. In literature, deformable models [3] and level sets [4] have become the most studied techniques for shape segmentation, due to their ability to adapt to the specific shape of the object of interest. These methods generally are too sensitive to the initial contour position and to the stop criterion. More robust algorithms have been proposed [5,6] in order to deal with those drawbacks, at the expense of a higher computational complexity.

In this paper, an extended version of [7], we describe a fast morphological segmentation approach that combines gray-scale information and prior shape knowledge. The method is easily parameterizable because it uses simple shape features. An overview of morphological segmentation is presented by Meyer in [8] where a unified framework for supervised or unsupervised, multi-scale or single scale, color or gray-scale and 2D or 3D images is introduced. Shape information has been used in mathematical morphology as attribute operators (connected filters [9]). Attribute operators compute criteria describing the shape or size of each connected component and then decide which components are preserved or discarded. Firstly, Vincent [10] presented area openings and then Breen and Jones [11] extended them to attribute openings (*AO*) and thinnings. Several applications have been developed using attribute filters such as: enhanced filtering [12], image compression [13] and image retrieval [14]. Maragos [15] proposed a multi-scale shape-size description using morphological opening and closing filters, named pattern spectrum, which is related to the notion of granulometries [16]. Urbach [17] extended them to shape pattern spectrum (shape granulometry), by using an attribute thinning as a shape operator. A geometric spectrum is presented in [18] for quantifying the geometric features on multidimensional binary images, which extends the work of Goutsias and Schonfeld [19]. They presented a morphological shape decomposition that uses a sequence of structuring elements and a sequence of set transformations. The obtained decomposition is called a generalized morphological segmentation.

Furthermore, a large number of segmentation methods exist to compute prior shape knowledge based on watershed [20–22]. They impose a priori shape knowledge, usually smoothness of the region contour, on the segmentation result. In [21], the snake energy criterion is used to merge over-segmented regions produced by the watershed while in [20], watershed segmentation is defined as an energy minimization. Hamarneh and Li [22] used k-means to incorporate shape knowledge before the segmentation stage. Besides, a new morphological operator, named ultimate opening (*UO*) [1], has been increasingly used as a powerful segmentation method due to its various advantages: non-parametric operator, segmentation of contrasted structures, intrinsically multi-scale, etc.

Our approach integrates the shape information into ultimate attribute opening *UAO*. In contrast to using only the difference of

☆ This paper has been recommended for acceptance by Sinisa Todorovic.

* Corresponding author. Tel.: +33 1 64694706.
E-mail addresses: jorge.hernandez@mines-paristech.fr (J. Hernández), beatriz.marcotegui@mines-paristech.fr (B. Marcotegui).

0262-8856/$ – see front matter © 2011 Elsevier B.V. All rights reserved.
doi:10.1016/j.imavis.2011.05.001

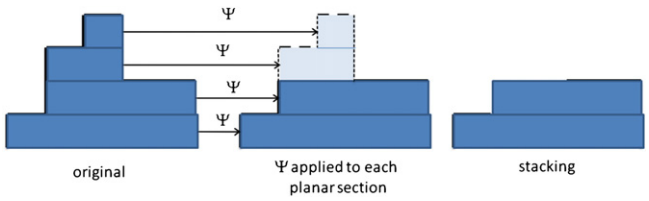

Fig. 1. Connected operator Ψ extended to functions: it applies to each planar section and stacks the results.

openings to locate regions, as done in the *UO*, the proposed method uses a similarity function defined through a prior knowledge of the shapes. This similarity function is based on the characteristics of the connected components *CC*s in images (shapes). Urbach et al. defined in [23] vector-attribute filters based on shape descriptors. They filter out *CC*s different from the prior one, based on a threshold on the vector distance. Our method combines the contrast with the attribute distance. Thus, contrasted shapes are extracted but favoring those which are shaped like the prior one. Experimental results are shown on real applications: facade analysis, scene-text detection and cell segmentation. In scene-text segmentation and cell segmentation, attribute histograms are analyzed in order to determine the main shape attributes. The method improves the result with respect to the classical *UAO*.

The paper is organized as follows. In Section 2, the theoretical background of connected operators, the *AO*, Salembier's max-tree and the *UO* are presented. Qualities and drawbacks of the *UO* are illustrated. Section 4 describes our method and introduces shape information into the *UO* Definition. In Section 5, experimental results are shown and the advantages of our method are illustrated. Finally, conclusions and future work are drawn in Section 6.

2. Theoretical background

In this section we introduce the ultimate attribute opening (*UAO*) operator, as well as some related aspects such as flat zones or the max-tree structure, used to implement the *UAO* efficiently. Let us consider X, a binary image on a space $E \subseteq Z^n$, and I a gray-scale image: $E \rightarrow Z$.

2.1. Flat zones and connected operators

Connected operators have been introduced by Serra and Salembier in [9]. These operators do not modify individual pixels, but act on connected components (*CC*), for binary images, or on flat zones (for gray level images). According to [9], a *CC* of a set, is a set of points that are connected by a path included in the set, while flat zones (*FZ*) of an image I are the largest *CC*s where the image is constant. We denote $FZ(I)$ the set of flat zones of image I.

Connected operators (Ψ) can only merge *FZ* but not break them into pieces. As a consequence, connected operators cannot add new boundaries, nor shift existing contours, but only simplify the image by removing contours. In other words, each *FZ* of the original image should be included in a single *FZ* of the resulting image: $\forall B \in FZ(I)$, $\exists C \in FZ(\Psi(I))/B \subset C$.

2.2. Attribute opening

Attribute openings (*AO*) are connected operators. For binary images, each *CC* of the original image is analyzed and an attribute is computed on it. Examples of attributes are the *CC* area, height or width of the bounding box or any other measure we can define on a given *CC* such as circularity (other examples can be found in [11]). An increasing criterion T is defined based on this attribute, usually in the form of a threshold on the attribute. A criterion T is said to be increasing if the fact that a set C satisfies T, implies that any other set B containing C satisfies T too. Then the *AO* of I is equal to the union of *CC* of I verifying the criterion T. For example, an area opening of size $\lambda(\gamma_\lambda^{area}(I))$ is equal to the union of *CC*s of I which area is greater than or equal to λ.

Attribute openings can be extended to gray level images by applying the transform to each planar section of the image $X_t(I)$, where $X_t(I) = \{x \in Z | I(x) \geq t\}$, and "stacking" the results $(X_t(\Psi(I)) = \Psi(X_t(I)))$ [9]. Fig. 1 illustrates this process. Thus, an attribute opening filters out peaks (bright regions), until the regional maximum verifies the criterion.

Fig. 2 shows a gray-scale image and two area openings, of sizes 100 and 500 pixels respectively. The regional maxima of these images are represented in blue. We can see that while the original image has many small maxima, the filtered images have larger and fewer maxima. The remaining maxima have an area of at least 100 and 500 pixels respectively, according to the corresponding opening size.

Efficient algorithms based on hierarchical queues [10], max-trees [24] and union find [25] have largely contributed to the diffusion of these operators. A comparison of these three methods has been presented in [26].

2.3. Ultimate opening

Ultimate opening (*UO*), has been introduced by Beucher in [1]. This is a non-parametric method and a non-linear scale-space based on morphological numerical residues to extract *CC*s. It analyzes the evolution of an image with a series of openings of increasing sizes: $\gamma_\lambda(I)$, $\lambda = \{0, 1, \ldots, N-1\}$ and N the maximum opening size considered. *UO* studies the series of residues between consecutive openings $r_\lambda(I) = \gamma_\lambda(I) - \gamma_{\lambda+1}(I)$ and keeps two significant outputs:

- $R_\theta(I)$, the maximal residue $r_\lambda(I)$. It is the strongest change generated by an opening. An important structure is supposed to be filtered out by this opening and the corresponding residue estimates its contrast.
- $q_\theta(I)$, the size of the opening leading to the maximal residue. If several openings lead to the same maximum $r_\lambda(I) = R_\theta(I)$, the

Fig. 2. Area openings (regional maxima in blue).

largest λ among them is chosen. $q_\theta(I)$ is set to 0 for pixels where all residues are null. This happens for the minimum of the image or for objects larger than N, the largest opening size considered.

According to Beucher [1], the definition describing the *UO* is written as:

Definition 1. *The ultimate opening operator, θ, of an image I is given by*:

$$\theta(I) : I \xrightarrow{\theta} (R_\theta(I), q_\theta(I)) \tag{1}$$

$$R_\theta(I) = max_\lambda(r_\lambda(I)) = max_\lambda(\gamma_\lambda(I) - \gamma_{\lambda+1}(I))$$
$$q_\theta(I) = \begin{cases} max\{\lambda + 1 | r_\lambda(I) = R_\theta(I)\} & R_\theta(I) > 0 \\ 0 & R_\theta(I) = 0 \end{cases} \tag{2}$$

where, γ_λ *is an opening of size* λ.

Beucher introduced *UO* with morphological openings. In this paper attribute openings (see Section 2.2) will be used instead, leading to ultimate attribute opening (*UAO*). *UAO* is a connected operator, that can be implemented efficiently on a max-tree structure (see Section 2.4). Fig. 3 shows three examples on real applications by using an ultimate height opening. The height is defined as the y-extent of a *CC*. The same non-parametric operator is applied on these images. The first example illustrates how the *UO* extracts internal structures (windows, doors, etc.) from facade images. In Fig. 3(b), we can appreciate the scene-text segmentation, by showing the operator powerfulness. Finally, a cell segmentation example is shown in Fig. 3(c). These applications will be further studied in Section 5.

Various applications have been developed using the *UO*: image analysis to measure the granulometry of rocks [27], automatic localization of text [28] and document image binarization [29]. *UAO* can be computationally expensive, if applied naively from its definition. Fabrizio in [30], proposes an efficient implementation based on the max-tree representation [24].

2.4. Max-tree

The max-tree, by duality min-tree, has been introduced by Salembier [24] as a structure to compute connected operators. Here

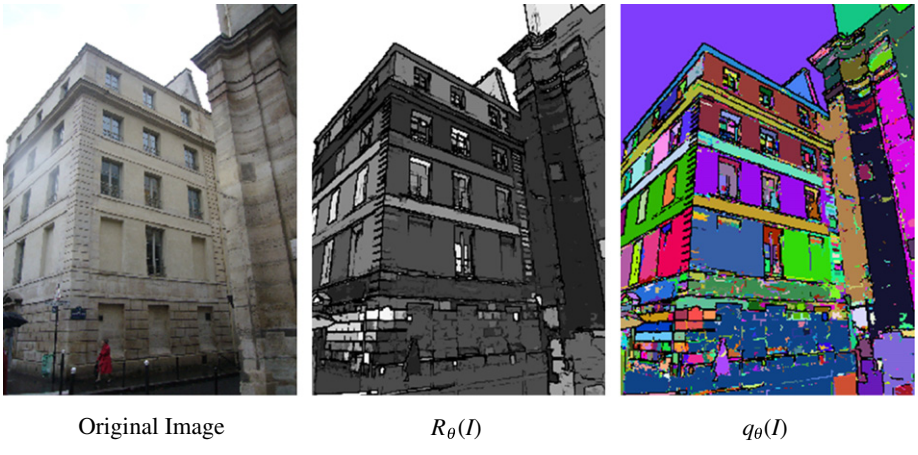

Fig. 3. Ultimate height opening on real images. N is equal to the vertical size of the image. $q_\theta(I)$ is represented in false colors in order to see the segmented regions.

we illustrate the concept of max-tree. For an exhaustive definition please refer to [24]. The max-tree is a tree, in the sense of graph theory, which gives a multi-scale representation of an image. Nodes represent the binary *CCs* of $X_t(I)$, the thresholded versions of image I at level t. Parent–child links describe inclusion relationships between the corresponding *CCs*. Thus, the root node corresponds to the whole image while leaf nodes correspond to the image maxima. One or several attributes, computed on *CCs*, can be associated with nodes, allowing an efficient computation of attribute openings. An example is presented in Fig. 4. The attribute κ used is the height (y-extent) of the associated *CC*. Root node, A_0^4, of level 0 and of height attribute $\kappa=4$ has two children B_1^3 at level 1 and C_2^3 at level 2, both with an attribute $\kappa=3$. Connected component C remains unchanged from $X_1(I)$ to $X_2(I)$. In that case, the maximum threshold for which the connected component is the same, is assigned to the node (level 2 in our example). Each branch leads to a leaf-node (E_5^1 and F_6^2) corresponding to the regional maxima of the image, at levels 5 and 6 respectively.

An attribute opening γ_λ removes nodes n of attribute $\kappa(n)$ smaller than λ. Fig. 5 shows the attribute opening results, with increasing λ values. These openings are obtained by pruning the tree at the corresponding dot-lines.

Fabrizio in [30] implemented a fast *UAO* on max-tree. The definition of the ultimate attribute opening involves a series of attribute openings (connected operators). Therefore, the max-tree is a suitable structure for its implementation [24]. Once the max-tree is computed, the different openings are obtained by simply pruning the tree nodes, with a simple threshold of their attribute. The residue between two consecutive openings is computed as the gray level difference of a node and the gray level of its first ancestor with a different attribute, as follows:

$$r_\lambda(child) = \begin{cases} t(child) - t(parent) & \kappa(parent) \neq \kappa(child) \\ t(child) - t(parent) + r_\lambda(parent) & \text{otherwise} \end{cases} \quad (3)$$

where *child* and *parent* are two linked nodes of the max-tree, $t(n)$ the gray level associated to node n and $\kappa(n)$ its corresponding attribute. Once these residues are computed, it is easy to compute the *UAO*, in a single upward tree traversal. Appendix A explains this process, as well as the step by step computation of *UAO* for Fig. 5.

3. Ultimate opening drawbacks

The *UO* presents several advantages as a segmentation method of homogeneous regions, such as non-parametric, intrinsically multi-scale and extraction of the most contrasted structures. However, the last advantage may be its biggest drawback. The *UO* is an operator without memory and it only saves the last maximum residue. It does not keep intermediate images, which could be also important. Retornaz describes this problem as an operator myopia [28]. *UO* problems are mainly produced by two configurations: nested structures and gradual transitions.

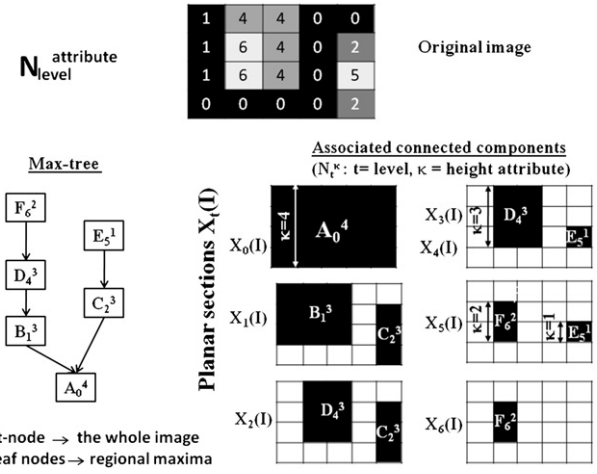

Fig. 4. Max-tree representation.

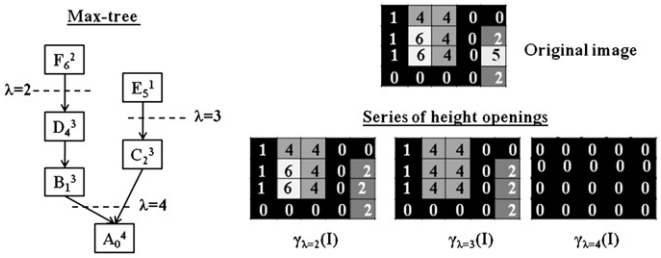

Fig. 5. Max-tree and height openings $\gamma_T(I)$, where T : $\kappa \geq \lambda$.

3.1. Nested structures

This problem appears when the interest structures are nested in other structures with a bigger contrast. Therefore, when a structure is contained in another, it may be masked by a bigger residue. For instance, a pyramidal configuration in the image is a typical case of the nested structures.

For example, in Fig. 6, a masking problem is illustrated by applying the ultimate attribute (height) opening. The synthetic image in Fig. 6(a) has three nested shapes: a rectangle (dimensions 120×40, $t=250$), a square (dimensions 30×30, $t=200$) and a circle (diameter 90, $t=175$). These structures are on a plateau of level $t=130$. Using Definition 1 with a height opening, step by step, we obtain the following results: the square is the first shape found ($\lambda=31$), and then this shape is masked by a circle filtered by opening $\lambda=91$. Before the height opening $\lambda=161$ is applied, two shapes have been detected; nevertheless, in this opening, an important residue masks relevant information.

3.2. Gradual transitions

Gradual transitions in the image produce small residues when an *UO* is carried out. For this reason, structures with gradual transitions and also nested in contrasted areas are likely to be masked. An example of this problem is shown in Fig. 7. Fig. 7(a) shows a synthetic image with a rectangle (dimensions 120×40, $t=250$) on a plateau of level $t=110$. The rectangle has a transition in the bottom (dimensions 2×40, $t=170$). This transition can be observed in Fig. 7(b). By using an ultimate height opening, the rectangle is masked by the plateau, because it has a residue of $250-170=80$ smaller than the plateau residue of 110.

In order to solve *UO* problems, we propose to incorporate shape information, exploiting a prior knowledge of the image and preserving specific shapes before being masked or/and merged.

3.3. Ultimate opening drawbacks on real images

Fig. 8 provides various examples of *UO* problems on real images. In Fig. 8(a), a lot of internal facade structures are masked. It is a problem of nested structures because the contrast between the wall and the windows is smaller than the contrast between the sky and the building facade. An example of gradual transitions is presented in Fig. 8(b). As it can be seen, all letters are masked because they have blurred boundaries, caused by the digitization process. Fig. 8(c) shows a gradual transition problem on cell images. Two cells are visibly separable but the operator merges both. An extended analysis of those problems on real images will be presented in Section 5.

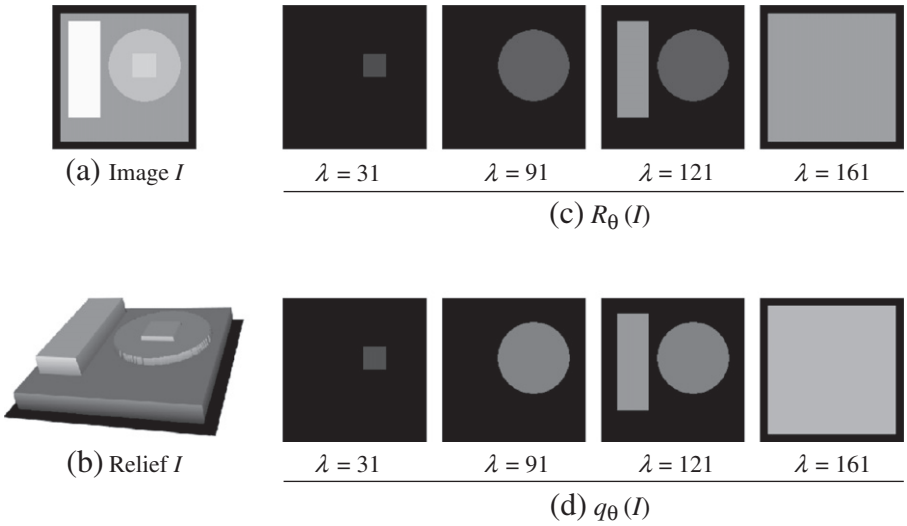

Fig. 6. Example: Masking problem produced by nested structures (a) Synthetic Image, (b) relief I representation, (c) and (d) intermediate images of $R_\theta(I)$ and $q_\theta(I)$, respectively.

4. Shape ultimate attribute opening

Shape ultimate attribute opening (*SUAO*) combines shape and gray-scale information in order to extract the most contrasted structures similar to a specific prior shape.

4.1. Shape information

In this section, we define our shape similarity measure in order to combine prior shape knowledge with the *UO* operator. The shape definition has been widely studied in the literature. Surveys of shape analysis methods can be found in [31–33].

In our context, we are interested in comparing two shapes (Ω_i, Ω_j) via a similarity function $\psi()$.

Most of the prior shape knowledge on segmentation approaches work on contours and a deformable model framework. In contrast, we propose to define a similarity function via shape attributes κ_Ω of regions, in order to favor specific shapes. In our method, the considered regions Ω, on which shape descriptors are computed, are the *CC*s associated with the max-tree nodes. We use the simplest shape descriptors: geometric features (height, width, etc.) and their relations (fill ratio, circularity, moments, etc.). Furthermore, more complex shape descriptors, such as Fourier moments or those based on multiple characteristics of a polygon form, can be used to describe shape information.

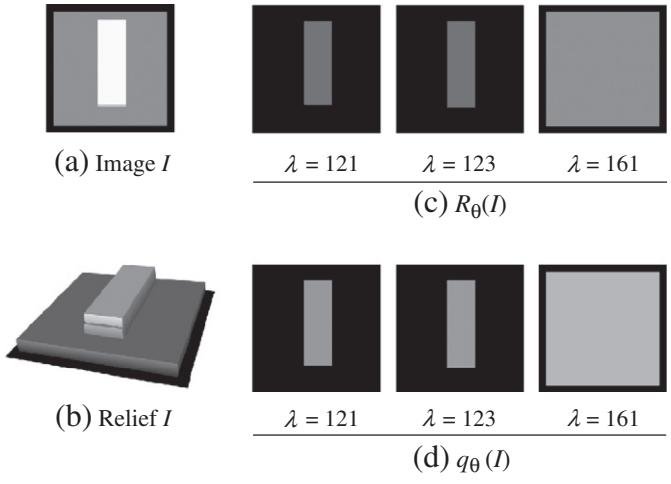

Fig. 7. Example: Masking problem produced by gradual transitions (a) synthetic image, (b) relief I representation, (c) and (d) intermediate images of $R_\theta(I)$ and $q_\theta(I)$, respectively.

Definition 2. *A similarity measure between two shapes, Ω_i and Ω_j, based on attribute κ, is defined as a function $\psi_\kappa : \Omega \times \Omega \rightarrow [0,1] \in \mathbb{R}$ verifying the following conditions*[34]:

- *Identity:* $\psi_\kappa(\Omega_i, \Omega_i) = 1$.
- *Uniqueness:* $\psi_\kappa(\Omega_i, \Omega_j) = 1$ *implies* $\kappa_{\Omega_i} = \kappa_{\Omega_j}$
- *Symmetry:* $\psi_\kappa(\Omega_i, \Omega_j) = \psi_\kappa(\Omega_j, \Omega_i)$

After having established these conditions, an example of similarity function ψ_κ is presented in Eq. 4:

$$\psi_\kappa\left(\Omega_i, \Omega_j\right) = \begin{cases} \left(1 - \dfrac{|\kappa_{\Omega_i} - \kappa_{\Omega_j}|}{\tau}\right)^{\varsigma} & |\kappa_{\Omega_i} - \kappa_{\Omega_j}| \le \tau \\ 0 & \text{otherwise} \end{cases} \tag{4}$$

where τ is the similarity threshold of attribute κ. The function reaches its maximum value when the difference between two shape attributes is zero ($\kappa_{\Omega_i} - \kappa_{\Omega_j} = 0$), the min value when the attribute difference is over a given threshold τ and a value in the interval [0,1] when $|\kappa_{\Omega_i} - \kappa_{\Omega_j}| < \tau$. ς determines if the dynamic range is wide ($\varsigma < 1$), linear ($\varsigma = 1$) or narrow (selective) ($\varsigma > 1$).

We have defined a similarity function with only one attribute κ. In practice, several measures are used to describe a prior shape in a same application. In that case a (simple) multiplication of similarity functions would be applied:

$$\psi = \prod_{\forall \kappa} \psi_\kappa\left(\Omega_i, \Omega_j\right). \tag{5}$$

All these possible shape attributes and similarity functions can be utilized to give an advantage to specific shapes in a segmentation process. Nevertheless, we must be careful with the selection of measures, because of the following reasons:

- *Computing time*: Measures are computed for each tree node. To keep a reasonable computing time, we have used the simplest shape attributes, because they can straightforwardly be estimated during the max-tree construction.
- *Invariance with respect to position, scale, and rotation*: The invariance of the proposed method depends on the chosen attributes. For example, the *UO* with a fill ratio attribute is not

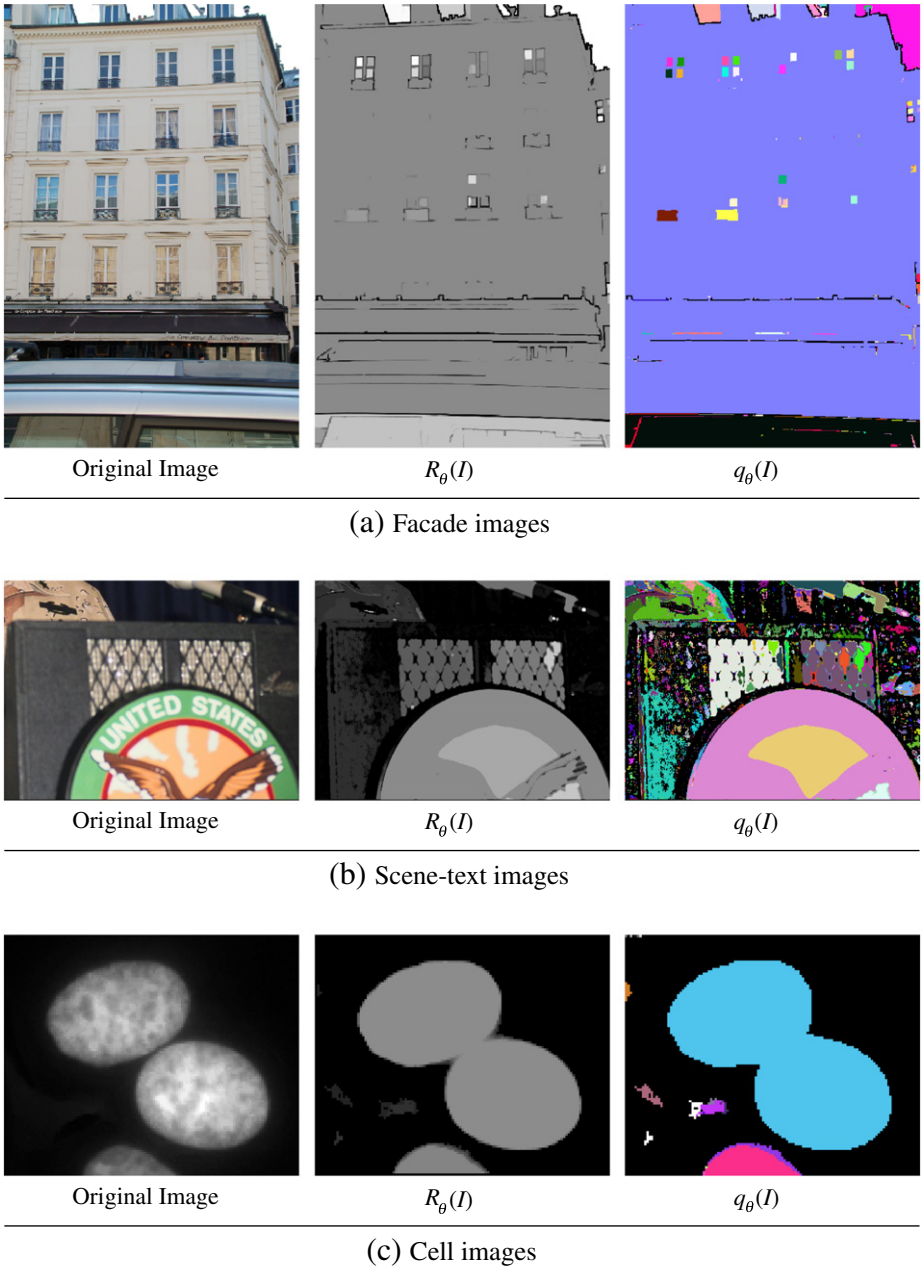

Fig. 8. Problems on real images.

rotation invariant, while if we choose the compactness descriptor, it will be fully invariant.

4.2. Shape ultimate opening

In this paper, we focus on attribute openings, that are connected operators. As explained in Section 2.4, each tree node corresponds to a *CC* of the image (see Fig. 4): the closer the node is to the root, the larger the *CC* is (according to the inclusion principle of the tree). We propose to rely on the *CC* associated to the nodes, named Ω in the following, in order to estimate the shape of the segmented regions.

We propose to consider a shape factor function $f(\Omega, \Omega_{ref})$ to a reference shape Ω_{ref} within the residue computation (Eq. 6). As Ω_{ref} is fixed, $f(\Omega, \Omega_{ref})$ is denoted by $f(\Omega)$.

$$r_\lambda^\Omega \leftarrow f(\Omega) r_\lambda \tag{6}$$

In that way, the residue of a Ω similar to Ω_{ref} is artificially increased, favoring its presence in the segmentation result, even if it is nested in a more contrasted shape different from the prior.

The shape factor function $f(\Omega)$ is related to the similarity function $\psi_{\forall\kappa}$ of Ω as follows: $1 + \alpha\psi_{\forall\kappa}$. An offset of 1 is added in order to switch to the standard *UO* when the similarity function is equal to 0 (r_λ^Ω becomes r_λ). As well, a multiplicative factor α is used to control the influence of the shape factor with respect to the gray level. Hence, $1+\alpha$ represents the maximum value that the function may reach. Finally, function f_Ω is stored on an image $F_\theta^\Omega(I)$ when the maximal residue ($R_\theta(I)$) is generated. With this information, we modify the original expression of the *UO* definition 1 by Definition 3.

Definition 3. *We define a shape ultimate opening θ^Ω of an image I by:*

$$\theta^\Omega(I) : I \xrightarrow{\theta^\Omega} \left(R_\theta^\Omega(I), q_\theta^\Omega(I), F_\theta^\Omega(I)\right) \tag{7}$$

$$R_\theta^\Omega(I) = \max_\lambda\left(r_\lambda^\Omega(I)\right) = \max_\lambda\left(f(\Omega)\times r_\lambda(I)\right) \tag{8}$$

$$q_\theta^\Omega(I) = \begin{cases} max\left\{\lambda+1 \,|\, r_\lambda^\Omega(I) = R_\theta^\Omega(I)\right\} & R_\theta^\Omega(I) > 0 \\ 0 & R_\theta^\Omega(I) = 0 \end{cases} \tag{9}$$

$$F_\theta^\Omega(I) = \begin{cases} f(\Omega) \,|\, r_\lambda^\Omega(I) = R_\theta^\Omega(I) & R_\theta^\Omega(I) > 0 \\ 0 & R_\theta^\Omega(I) = 0 \end{cases} \tag{10}$$

where, Ω is a CC associated with a tree node (see Fig. 4) and $f(\Omega)$ is a shape factor function. $F_\theta^\Omega(I)$ gives the similarity of segmented regions with the reference shape.

As it can be seen, the shape factor is directly applied on the residue computation, artificially increasing the residue of regions similar to the prior one.

4.3. Example on synthetic image

We test our approach on a synthetic image (Fig. 6(a)). First, we try to favor rectangular shapes. For this purpose, we use as a shape metric the fill ratio $\Upsilon_\Omega = \frac{A_\Omega}{Abbox_\Omega}$, where (A_Ω) is the shape area and $(Abbox_\Omega)$ is the bounding box area. The ratio lies in the range [0,1]; where, if the value is close to 1, it means that the shape corresponds to a rectangular polygon without rotation, i.e. $\Upsilon_{\Omega_{ref}} = 1$. Then, we have imposed an area limit (90% of image area A_I) to validate the shape in order to reject the largest regions. This factor function is translated into Eq. 11.

$$\begin{aligned} & f(\Omega) = 1 + \alpha\psi_{\kappa_1}(\Omega)\ \psi_{\kappa_2}(\Omega) \\ \text{where,}\ & \alpha = max(I)/2, max = 255 \\ & \psi_{\kappa_1}(\Omega) = \Upsilon_\Omega \\ & \psi_{\kappa_2}(\Omega) = \begin{cases} 1 & A_\Omega < 90\%A_I \\ 0 & \text{otherwise} \end{cases}. \end{aligned} \tag{11}$$

Fig. 9 presents the result on a synthetic image. In this case, the masking problem is solved and the three shapes are segmented. The importance of limit $\psi_{\kappa_2}(\Omega)$ is remarkable in this example, because the masking shape has a high fill ratio $\Upsilon_\Omega \approx 1$. Using the limit, the shape has a factor equal to 1, thus $r_\lambda^\Omega = r_\lambda$.

Even though Υ mainly favors rectangular structures, the circular shape factor is high enough to unmask it. If we want to be more selective, we modify $\psi_{\kappa_1}(\Omega)$ by a narrower function. For example, we change Υ_Ω in Eq. 11 by Υ_Ω^3 (Eq. 12).

$$\begin{aligned} & f(\Omega) = 1 + \alpha\psi_{\kappa_1}(\Omega)\ \psi_{\kappa_2}(\Omega) \\ \text{where,}\ & \alpha = \max(I)/2, \max = 255 \\ & \psi_{\kappa_1}(\Omega) = (\Upsilon_\Omega)^3 \\ & \psi_{\kappa_2}(\Omega) = \begin{cases} 1 & A_\Omega < 90\%A_I \\ 0 & \text{otherwise} \end{cases}. \end{aligned} \tag{12}$$

Another shape factor example is implemented to favor circular shapes using as a shape metric the circularity measure $\frac{4\pi A_\Omega}{(L_\Omega)^2}$, with A the area and L the perimeter of Ω. Eq. 13 shows a factor function by using the circularity expression. Figs. 10(c) and 11(c) confirm that rectangles and circles are segmented, respectively.

$$\begin{aligned} & f(\Omega) = 1 + \alpha\psi_{\kappa_1}(\Omega) \\ \text{where,}\ & \alpha = \max(I)/2 \\ & \psi_{\kappa_1}(\Omega) = \frac{4\pi A_\Omega}{(L_\Omega)^2} \end{aligned} \tag{13}$$

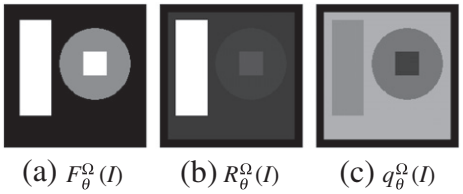

(a) $F_\theta^\Omega(I)$ (b) $R_\theta^\Omega(I)$ (c) $q_\theta^\Omega(I)$

Fig. 9. *SUAO* of Fig. 6(a)) with Eq. 11 as factor function.

(a) $F_\theta^\Omega(I)$ (b) $R_\theta^\Omega(I)$ (c) $q_\theta^\Omega(I)$

Fig. 10. *SUAO* of Fig. 6(a) with Eq. 12 as factor function.

5. Applications

In order to demonstrate the performance of our method, we illustrate three segmentation applications: facade image analysis, scene-text detection and cell segmentation. All databases and result tests are available on the following web site: http://cmm.ensmp.fr/~hernandez/uo_en.html.

5.1. Facade image analysis

We focus on a segmentation procedure behind the facade modeling [35,36] to detect/extract structural objects, mainly windows. This facade analysis has been developed in the framework of Cap Digital Business Cluster TerraNumerica project (http://cmm.ensmp.fr/TerraNumerica) which aims at increasing the productivity and the realism of urban modeling.

Initially, we employed an ultimate attribute opening to segment facade images. For the facade structure detection, a height attribute of the *CCs* is used. Fig. 12 shows an example of *UAO* and *SUAO* using HSL color gradient [37]. In the example, most internal structures are masked in the segmentation process due to the fact that the contrast between the sky and the facade is bigger than the contrast between the wall and the windows (Fig. 12(c)). Most urban images contain sky information and high contrast roof-wall; for those reasons the *UAO* segmentation is highly affected by the masking problem.

In facade images, windows and doors are at least partially rectangular. Mayer and Reznik [38] propose fill ratio (Υ_Ω) and aspect ratio $(\aleph_\Omega = \frac{height}{width})$ as features to discriminate them. They state that the aspect ratio of a window generally lies between 0.2 and 5.0. With these features, we define the similarity function:

$$\begin{aligned} & f(\Omega) = 1 + \alpha\psi_{\kappa_1}(\Omega)\ \psi_{\kappa_2}(\Omega) \\ & \psi_{\kappa_1}(\Omega) = (\Upsilon_\Omega)^2 \\ & \psi_{\kappa_2}(\Omega) = \begin{cases} (\aleph_\Omega)^{0.5} & \aleph_\Omega > 0.2 \\ 0 & \text{otherwise} \end{cases}. \end{aligned} \tag{14}$$

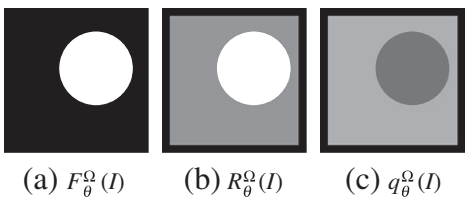

(a) $F_\theta^\Omega(I)$ (b) $R_\theta^\Omega(I)$ (c) $q_\theta^\Omega(I)$

Fig. 11. *SUAO* of Fig. 6(a) with Eq. 13 as factor function.

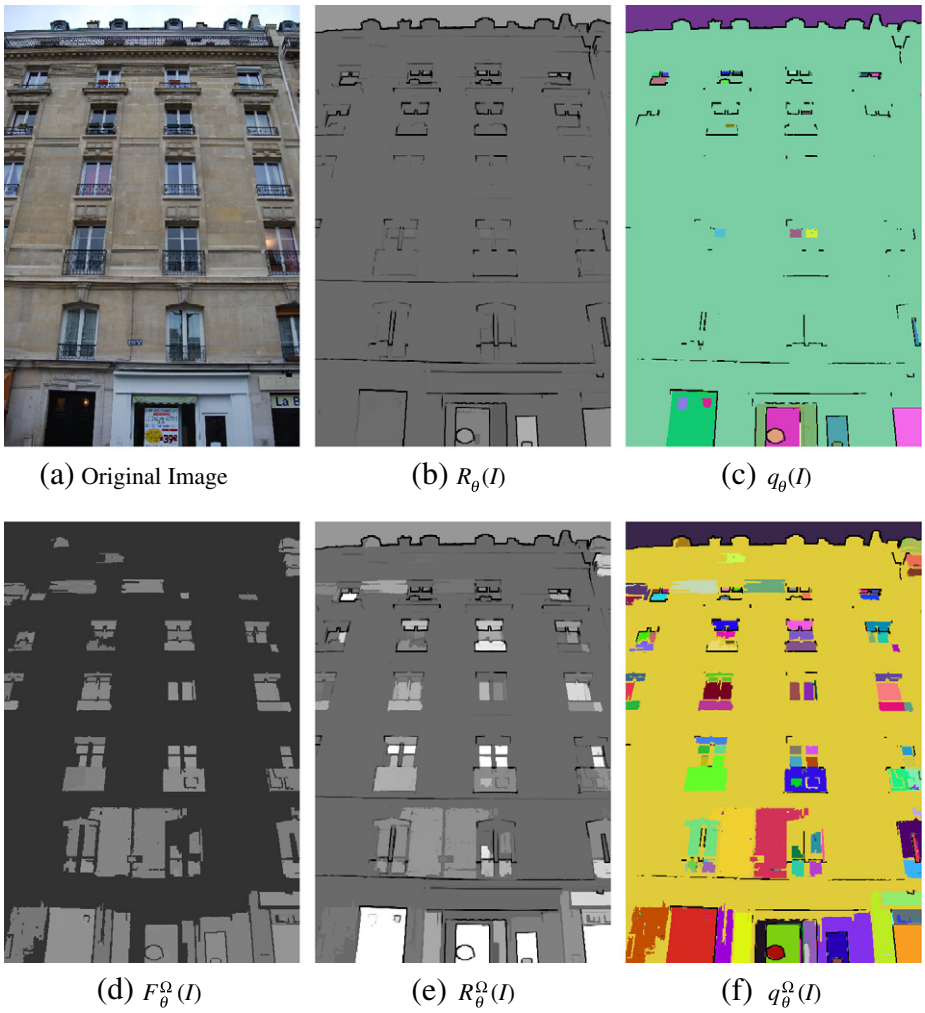

Fig. 12. (a) Original image, (b)–(c) R_θ (I) and q_θ (I) of *UAO*, (d)–(f) F^Ω_θ (I), R^Ω_θ (I) and q^Ω_θ (I) of *SUAO*.

The first shape attribute is fill ratio ($\kappa_1 = \Upsilon_\Omega$). We have used a square value $\varsigma = 2$ as narrow dynamic function to be more selective. The second shape attribute κ_2 is an aspect ratio $\aleph$. The standard aspect ratio (h/w) is too sensitive to small width variations, moreover it does not validate shape similarity conditions (see Section 4.1). Thus, we have computed $\aleph = \frac{min(h,w)}{max(h,w)}$. We have used a wide dynamic function $\varsigma = 0.5$ and truncated on $\aleph > 0.2$. After several tests with facade images, the biggest gradient in a facade is about ten times bigger than the one between the wall and the windows. For this reason, we have chosen $\alpha = 9$, i.e. $1 + \alpha = 10$.

The segmentation result on the facade image is illustrated in Fig. 12(f). Our approach shows a better segmentation because most structures of interest are correctly segmented.

To illustrate the robustness of the shape factor to perspective effects, Fig. 13 shows the shape factor for a window turning around its

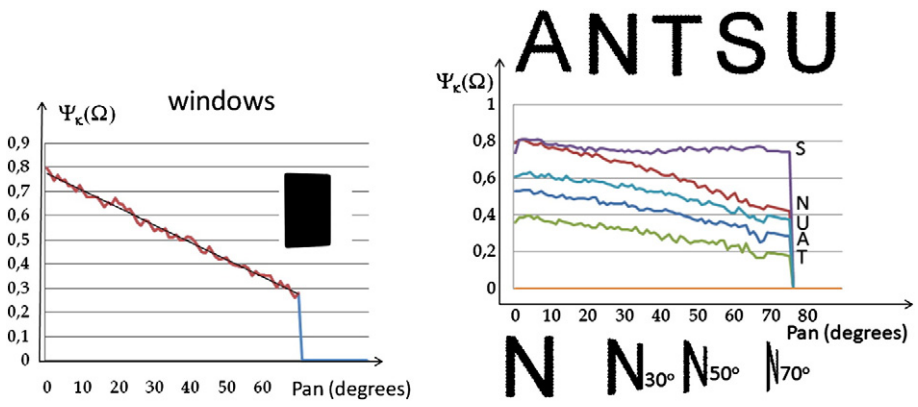

Fig. 13. Shape factor evolution with pan angle (rotation around the Z-axis), for windows (left) and letters (right).

(a) Original Image (b) $F_\theta^\Omega(I)$ (c) $R_\theta^\Omega(I)$ (d) $q_\theta^\Omega(I)$

Fig. 14. (a) Original image [39], (b)–(d)$F_\theta^\Omega(I)$, $R_\theta^\Omega(I)$ and $q_\theta^\Omega(I)$ of *SUAO*.

Z-axis in a view frustum (pan angle from 0° to 80°). The shape factor decreases when the perspective increases. However, it is still of about 0.5 for 40° of panning. Fig. 14 shows an example on a real image, illustrating the good detection of windows even with non fronto-parallel facades.

5.2. Scene-text detection

The text in a scene is linked to the semantic context of the image and constitutes a relevant descriptor for content-based image indexing [28]. This research has been developed as part of iTOWNS (Image-based Town On-line Web navigation and Search Engine, http://www.itowns.fr/) project. The goal of this project is to develop a new generation of multimedia web tools that combine a 3D geographic browser with an image-based search engine based on a data indexing images and visual context.

In several cases, the text on images is at least partially placed on a surface of different colors, such as placards, posters, etc.; and favors the visibility of letters. But this surface is also contrasted in comparison to its surroundings (Figs. 15(a) and 16(a)). When we utilize the *UAO*, characters may be masked by the contrast of the signboard with its surroundings. In the same way, we propose some text features to define shape information. Based on histograms of approximately 5000 analyzed characters, letter features are described as follows: 1 — 97% of letters have an aspect ratio bigger than 0.4, 2 — 84% of letters fall approximately between 0.2 and 0.9 fill ratio and 3 — the biggest height (resp. width) of a character is 1/3 of the image height H_I (resp. width W_I). We have used a similarity function analogous to facade application. For κ and Υ metrics, wide dynamic functions have been used. For Υ attribute, we have used a centred function on $\Upsilon_{ref}=0.55$ and a threshold $\tau=\pm0.35$ leading to the required limits $\Upsilon_\Omega\in(0.2, 0.9)$ (Eq.15). Fig. 13 shows the evolution of this factor with a pan angle, for different letters. Some letters, such as S or N, have a high shape factor, that decreases slowly with a pan angle. Thus, the residue of these letters is boosted to be present in the result. Other letters, those with smaller fill ratio such as T, have a smaller shape factor, specially with large pan angles. In that case, the combination of contrast and shape factor is required to select significant *CC*s.

$$f(\Omega) = 1 + \alpha\psi_{\kappa_1}(\Omega)\ \psi_{\kappa_2}(\Omega)\ \psi_{\kappa_3}(\Omega)$$

where, $\alpha = 9$

$$\psi_{\kappa_1}(\Omega) = \begin{cases} (\kappa_\Omega)^{0.5} & \kappa_\Omega > 0.4 \\ 0 & \text{otherwise} \end{cases}$$

$$\psi_{\kappa_2}(\Omega) = \begin{cases} \left(1-\left(\dfrac{\Upsilon_\Omega-0.55}{0.35}\right)\right)^{0.5} & 0.2 < \Upsilon_\Omega < 0.9 \\ 0 & \text{otherwise} \end{cases} \quad (15)$$

$$\psi_{\kappa_3}(\Omega) = \begin{cases} 1 & h_\Omega < \dfrac{H_I}{3} \wedge w_\Omega < \dfrac{W_I}{3} \\ 0 & \text{otherwise} \end{cases}.$$

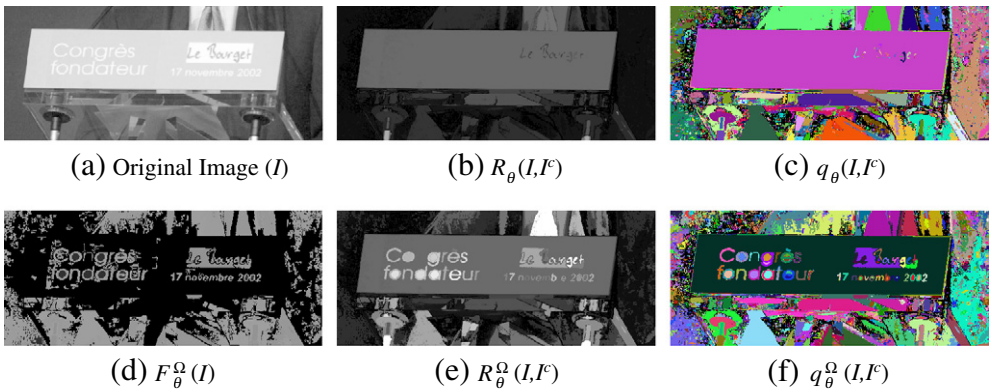

(a) Original Image (*I*) (b) $R_\theta(I,I^c)$ (c) $q_\theta(I,I^c)$

(d) $F_\theta^\Omega(I)$ (e) $R_\theta^\Omega(I,I^c)$ (f) $q_\theta^\Omega(I,I^c)$

Fig. 15. (a) Original image, (b)–(c)$R_\theta(I, I^c)$ and $q_\theta(I, I^c)$ of *UAO*, (d)–(f) $F_\theta^\Omega(I, I^c)$, $R_\theta^\Omega(I, I^c)$ and $q_\theta^\Omega(I, I^c)$ of *SUAO*.

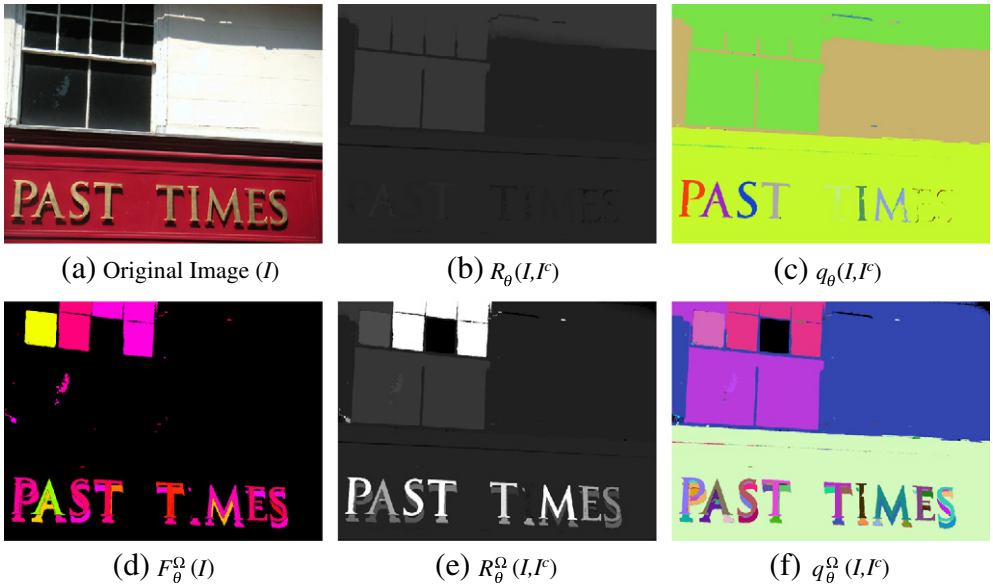

Fig. 16. (a) Original image, (b)–(c)$R_\theta(I, I^c)$ and $q_\theta(I, I^c)$ of *UAO*, (d)–(f) $F^\Omega_\theta(I, I^c)$, $R^\Omega_\theta(I, I^c)$ and $q^\Omega_\theta(I, I^c)$ of *SUAO*.

Besides, scene text may be light or/and dark. In order to deal with both polarities the *UO* is applied to the image and to its inverse. For each pixel, the polarity leading to a bigger residue is kept (see Eq. 16).

$$\begin{aligned} R_\theta(I,I^c) &= max(R_\theta(I), R_\theta(I^c)) \\ q_\theta(I,I^c) &= \begin{cases} q_\theta(I) & R_\theta(I) > R_\theta(I^c) \\ q_\theta(I^c) & \text{otherwise} \end{cases} . \end{aligned} \tag{16}$$

Figs. 15 and 16 show the results of the text detection using the *UAO* and the *SUAO* of a placard image. Using *UAO*, most letters have been masked. With our method, the masking problem is avoided and all letters become visible (Figs. 15(f) and 16(f)). As well, we obtain a homogenous value on the whole placard surface. The results from this study indicate that the proposed method is superior to the classical *UAO* segmentation.

5.3. Segmentation of cell images

The recent emergence of high-throughput automated image acquisition technologies has changed forever the way cell biologists collect and analyze data [40]. The interpretation of cellular phenotypes is now a major investigation subject in biology. Thus, the development of automated methods which aim at identifying novel and biological relevant phenotypes is a major challenge. For instance, blocking a gene with a RNA interference (RNAi) may highlight this gene effect over the cell normal functioning. The observation of a toxic molecule may show new action modes and put on the right track to develop new medicines. This study is carried out within the framework of RAMIS (Rock Analysis Module and Interface for Screening) project of Cancer-Bio-Health Cluster of Toulouse-France. An image collection acquired by multi-parametric cell labeling and automated cell image methods is analyzed.

In image processing, the morphological (size, shape, texture, etc.) properties of cells provide valuable information worth exploring by starting with a segmentation step. We propose as a segmentation approach the *UAO* operator. However, the use of this operator presents several drawbacks, such as a masking problem produced by gradual transition associated with blur and cell proximity and undesirable nuclei over-segmentation. By analyzing histograms of approximately 1200 cells, the cell features are described as follows: 1 — circularity is the principal attribute, 2 — area (A) falls approximately between 500 and 3000 pixels and 3 — cells height (h) and width (w) lie between 15 and 110 pixels. Eq. 17 shows the resulting shape factor function:

$$\begin{aligned} & f(\Omega) = 1 + \alpha \psi_{\kappa_1}(\Omega)\ \psi_{\kappa_2}(\Omega)\ \psi_{\kappa_3}(\Omega) \\ & \text{where}\quad \alpha = 10, \psi_{\kappa_1}(\Omega) = \frac{4\pi A_\Omega}{(L_\Omega)^2} \\ & , \psi_{\kappa_2}(\Omega) = \begin{cases} 1 & 500 \text{ b } A_\Omega \text{ b } 3000 \\ 0 & \text{otherwise} \end{cases} \\ & \psi_{\kappa_3}(\Omega) = \begin{cases} 1 & h_\Omega \text{ and } w_\Omega \in (15, 110) \\ 0 & \text{otherwise} \end{cases} . \end{aligned} \tag{17}$$

Fig. 17 shows the comparison between the *UAO* and the *SUAO*. Note that $q_\theta(I)$ and $q^\Omega_\theta(I)$ present a lot of noisy *CCs*. Thus, once the *SUAO* is performed, a coarse elimination of *CCs* is carried out. A global threshold (t = 2) of average $R_\theta(I)$ on $q_\theta(I)$ is applied in order to remove low contrasted structures. With the coarse filter most noisy *CCs* are eliminated. Both segmentations are similar (Fig. 17(d) and (h)). However, the *SUAO* has unmasked several cells on the right-down region and has separated some linked cells. Our approach cannot avoid a leakage problem when leak between two cells happens before *CCs* have a high factor. Besides, it reduces nuclei segmentation by favoring the whole cell structure. Nevertheless, when a nuclei is slightly circular, it is favored too. Experimental results indicate that the proposed approach can be used to segment cells for further analysis by reducing the problems of the classical *UAO*.

6. Conclusion and future work

A novel segmentation method based on the ultimate attribute opening (*UAO*), combined with shape information, is introduced in this paper. It consists in reinforcing the contrast of regions which are shaped like the prior one. An efficient implementation based on the max-tree representation is proposed. In order to estimate the shape of segmented regions, we rely on the *CCs* associated to tree nodes. The independence of the residue and the shape descriptor computation allow the use of any shape distance in the proposed framework. Our approach focuses on particle segmentation [41] and it is not suitable for highly textured regions.

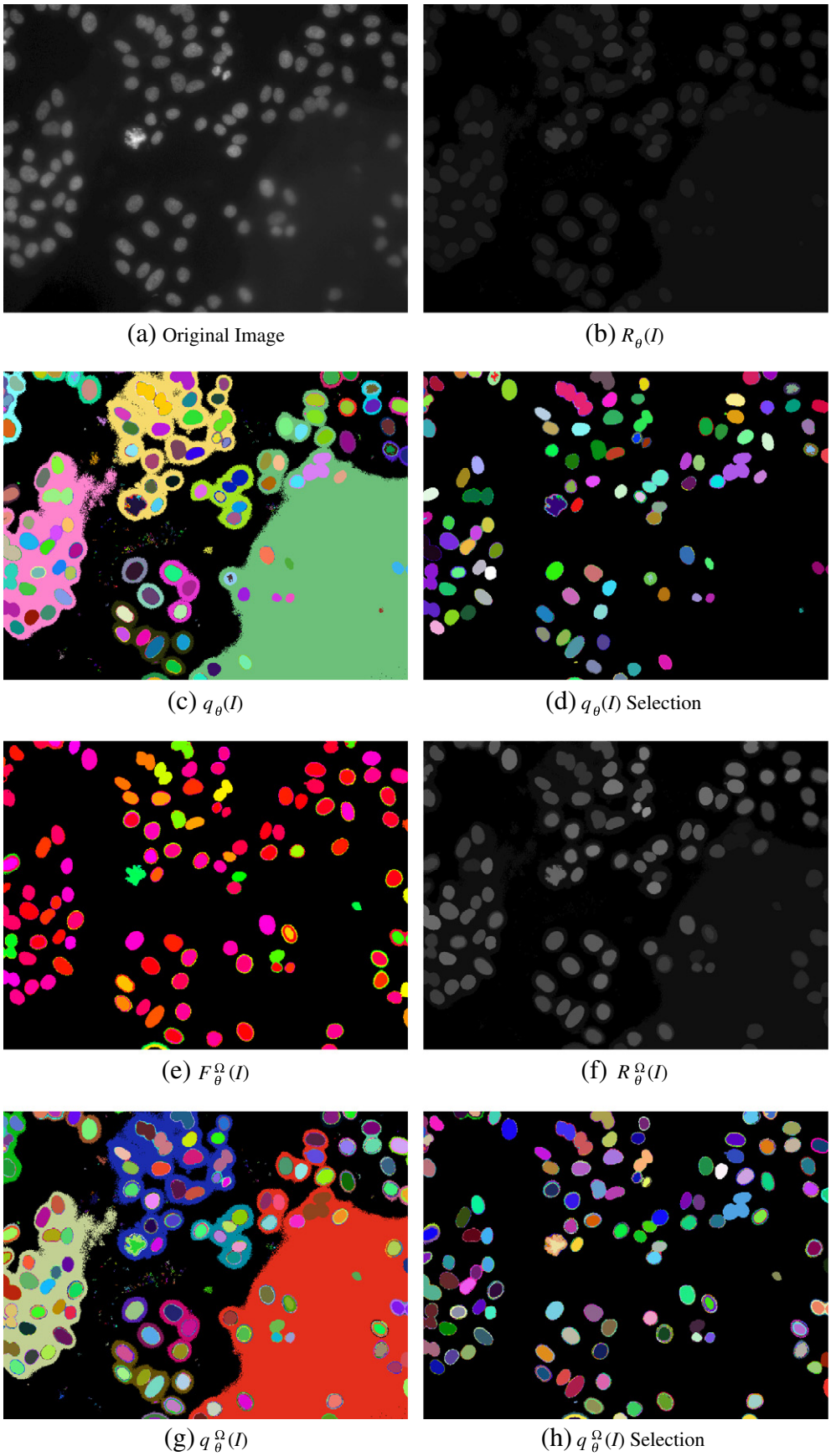

Fig. 17. (a) Original image: sample RNAi fluorescent images, (b)–(d) R_θ (I) q_θ (I) and q_θ (I) + coarse elimination of *UAO*, (e)–(h) F^Ω_θ (I), R^Ω_θ (I), q^Ω_θ (I) and q of *SUAO*.

Much better segmentation results, compared to the standard *UAO*, are reported and many other examples can be seen in our website [1]. The use of very simple shape descriptors, such as fill ratio or aspect ratio, significantly improves the results for a given application, with a marginal increase in the computation time. The approach has been validated in three applications: 1. facade, 2. text and 3. cell segmentation. A benchmark with other state of the art methods would be interesting, but as far as we know there is no annotated database with objects of a given shape. The creation of such a database is a tedious work, out of the scope of this paper.

The *UAO* provides two pieces of information, contrast ($R_\theta^\Omega(I)$) and size ($q_\theta^\Omega(I)$). The proposed method provides a third interesting piece of information: the shape factor image ($F_\theta^\Omega(I)$), that conveys a shape similarity measure with a reference shape.

In the future, we will analyze in detail the shape factor image. The detection process is the first step in computer vision problems. We intend to apply a machine learning process using shape features (together with color descriptors) to classify regions in the three applications. Furthermore, machine learning techniques could be introduced as a factor function into the presented method. For example, machine learning techniques can be used to estimate the probability of regions to belong to a given class. This probability can be used to weigh the original residues, favoring the segmentation of regions of the given class.

Acknowledgments

The work reported in this paper has been performed as part of Cap Digital Business Cluster Terra Numerica project, iTOWNSs project and RAMIS project.

Appendix A. *UAO* computation on max-tree

Fig. A.18 shows max-tree computation of the *UAO*. When pruning the tree, all regions corresponding to the nodes of the branch are merged in a single region. This region becomes indivisible for larger openings. Hence, removing a node produces a residue for all pixels of its descendant nodes. For this reason, an upward tree analysis, from the root to the leaves, allows to efficiently propagate the residual information, as it has been described in [30]. Instead of computing for each node the maximum (required for the *UAO* computation) between its residue and the residue of all its ancestors, an ancestor transmits its residue to its children, and the maximum residue (R_θ) of all nodes is computed in a single tree traversal.

The process starts at the root node: $R_\theta(root)$ and $q_\theta(root)$ are initialized to zero, and propagated to root children. Every child computes its own residue, according to Eq. 3 and compares it with $R_\theta(parent)$. $R_\theta(child)$ keeps the maximum value between them. q_θ is defined as the size of the opening producing the maximum residue. If $r(child) > R_\theta(parent)$, q_θ keeps the child attribute ($\kappa(child)+1$). Otherwise, R_θ and q_θ are propagated ($R_\theta(child) = R_\theta(parent)$ and $q_\theta(child) = q_\theta(parent)$). Each child becomes parent and repeats the process. Let us see step by step this process on a simple tree, the one of Fig. 4.

- B_1^3, D_4^3 and C_2^3 are CCs with an attribute $\kappa = 3$. Then they are modified by γ_4 opening ($\lambda = \kappa + 1 = 4$), generating the following residues: $r_4(C_2^3) = 2 - 0 = 2$, $r_4(B_1^3) = 1 - 0 = 1$ and $r_4(D_4^3) = 4 - 0 = 4$. These residues are the first ones computed, so all of them are maximum and $R_\theta(C_t^\kappa)$ is set to $r_4(C_t^\kappa)$ and $q_\theta(C_t^\kappa)$ is set to $4 = \kappa(C_t^\kappa) + 1$ for the three nodes (B_1^3, D_4^3 and C_2^3).

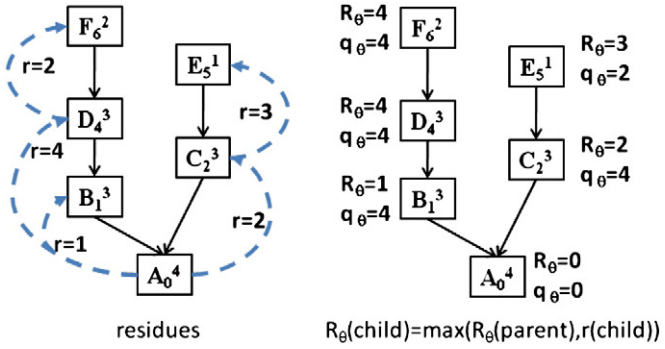

Fig. A.18. *UAO* computation on max-tree.

- Opening γ_3 cuts $F_6^2 \mapsto D_4^3$ branch, producing a residue $r_3(F_6^2) = 6 - 4 = 2$, which is smaller than the parent residue. Thus, the parent residue is propagated: $R_\theta(F_6^2) = max(R_\theta(D_4^3), r_3(F_6^2)) = max(4, 2) = 4$ and $q_\theta(F_6^2) = 4$.
- Opening γ_2 cuts $E_5^1 \mapsto C_2^3$ branch, producing a residue 5-2 = 3. This residue is bigger than the parent residue, updating $R_\theta(E_5^1) = max(R_\theta(C_2^3), r_2(E_5^1)) = max(2, 3) = 3$ and $q_\theta(E_5^1) = \kappa(E_5^1) + 1 = 2$.

As mentioned before, a node residue is computed as the difference of its gray level and the gray level of its first ancestor with a different attribute (and not with the gray level of its direct parent). An example of this situation can be seen on the left branch of the tree. The residue of node D_4^3 is not 3, ($D_4^3 - B_1^3 = 4 - 1 = 3$) but 4, ($D_4^3 - A_0^4$). This residue can be computed on the tree in a recursive procedure, following Eq. 3. In this case, $r_4(D_4^3) = (4 - 1) + (1 - 0) = 3 + 1 = 4$.

References

[1] S. Beucher, Numerical residues, Image Vision Comput. 25 (4) (2007) 405–415.
[2] R.C. Gonzalez, R.E. Woods, Digital Image Processing, 3rd Ed. Prentice-Hall, Inc., Upper Saddle River, NJ, USA, 2006.
[3] M. Kass, A. Witkin, D. Terzopoulos, Snakes: active contour models, Int. J. Comput. Vision 1 (4) (1988) 321–331.
[4] S. Osher, J.A. Sethian, Fronts propagating with curvature-dependent speed: algorithms based on Hamilton–Jacobi formulations, J. Comput. Phys. 79 (1) (1988) 12–49.
[5] D. Mumford, J. Shah, Optimal approximations by piecewise smooth functions and associated variational problems, Commun. Pure Appl. Math. 42 (5) (1989) 577–685, doi:10.1002/cpa.3160420503.
[6] T.F. Chan, L.A. Vese, Active contours without edges, IEEE Trans. Image Process. 10 (2) (2001) 266–277, doi:10.1109/83.902291.
[7] J. Hernández, B. Marcotegui, Ultimate attribute opening segmentation with shape information, Proc. of the 9th Intern. Symposium on Mathematical Morphology and Its Application to Signal and Image Processing, ISMM '09, Springer-Verlag, 2009, pp. 205–214.
[8] F. Meyer, An overview of morphological segmentation, Int. J. Pattern Recognit Artif Intell. 15 (7) (2001) 1089–1118.
[9] P. Salembier, J. Serra, Flat zones filtering, connected operators, and filters by reconstruction, IEEE Trans. Image Process. 4 (1995) 1153–1160.
[10] L. Vincent, Y.-L. O, A. Toet, D. Foster, H.J.A.M. Heijmans, P. Meer, Morphological area openings and closings for grey-scale images, Proc. of the Workshop "Shape in Picture", 7–11 September 1992, Driebergen, Springer, Berlin, The Netherlands, 1994, pp. 197–208.
[11] E.J. Breen, R. Jones, Attribute openings, thinnings, and granulometries, Comput. Vision Image Understanding 64 (3) (1996) 377–389.
[12] M.H.F. Wilkinson, M.A. Westenberg, Shape preserving filament enhancement filtering, Medical Image Computing and Computer-Assisted Intervention, volume 2208 of Lecture Notes in Computer Science, 2001, pp. 770–777.
[13] F. Tushabe, M.H.F. Wilkinson, Image preprocessing for compression: attribute filtering, inproceedings World Congress on Engineering & Computer Science 2007, 2007, pp. 999–1005.
[14] E.R. Urbach, J.B.T.M. Roerdink, M.H.F. Wilkinson, Connected shape-size pattern spectra for rotation and scale-invariant classification of gray-scale images, IEEE Trans. Pattern Anal. Mach. Intell. 29 (2) (2007) 272–285.
[15] P. Maragos, Pattern spectrum and multiscale shape representation, IEEE Trans. Pattern Anal. Mach. Intell. 11 (7) (1989) 701–716.
[16] G. Matheron, Random Sets and Integral Geometry, John Wiley & Sons, New York, 1975.

[1] http://cmm.ensmp.fr/~hernandez/uo_en.html

[17] E. Urbach, M. Wilkinson, Shape-only granulometries and gray-scale shape filters, Proc. of the 2nd Proc. of the eight Intern. Symposium on Mathematical Morphology, ISMM '02, 2002, pp. 305–314.
[18] F.Y. Shih, C.C. Pu, Morphological shape description using geometric spectrum on multidimensional binary images, Pattern Recognit. 25 (9) (1992) 921–927.
[19] D. Schonfeld, J. Goutsias, Robust morphological representation of binary images, Proc. of the "Intern. Conf. on Acoustics, Speech, and Signal Processing", 3–6 April 1990, Albuquerque, New Mexico, IEEE, New York, NY, U.S.A, 1990, pp. 2065–2068.
[20] J. Park, J.M. Keller, Snakes on the watershed, IEEE Trans. Pattern Anal. Mach. Intell. 23 (10) (2001) 1201–1205.
[21] H. Nguyen, M. Worring, R. van den Boomgaard, Watersnakes: energy-driven watershed segmentation, IEEE Trans. Pattern Anal. Mach. Intell. 25 (3) (2003) 330–342.
[22] G. Hamarneh, X. Li, Watershed segmentation using prior shape and appearance knowledge, Image Vision Comput. 27 (1–2) (2009) 59–68.
[23] E.R. Urbach, N.J. Boersma, M.H. Wilkinson, Vector-attribute filters, Proc. of the 7th Intern. Symposium on Mathematical Morphology, ISMM '05, 2005, pp. 95–104.
[24] P. Salembier, A. Oliveras, J.L. Garrido, Anti-extensive connected operators for image and sequence processing, IEEE Trans. Image Process. 7 (1998) 555–570.
[25] M.H.F. Wilkinson, J.B.T.M. Roerdink, Fast morphological attribute operations using Tarjan's union-find algorithm, Proc. Intern. Symposium on Mathematical Morphology, ISMM '00, Kluwer, 2000, pp. 311–320.
[26] A. Meijster, M. Wilkinson, A comparison of algorithms for connected set openings and closings, IEEE Trans. Pattern Anal. Mach. Intell. 24 (4) (2002) 484–494.
[27] S. Outal, Quantification par analyse d'images de la granulométrie des roches fragmentées: amélioration de l'extraction morphologique des surfaces, amélioration de la reconstruction stéréologique, Ph.D. thesis, CMM/GEOSCIENCES - École Mines Paris (June 2006).
[28] T. Retornaz, Détection de textes enfouis dans des bases d'images généralistes. un descripteur sémantique pour l'indexation., Ph.D. thesis, École des Mines de Paris (2007).
[29] J. Hernández, B. Marcotegui, Document image binarization using ultimate attribute opening, Tech. rep., CMM-Mines ParisTech, 2009.
[30] J. Fabrizio, B. Marcotegui, Fast implementation of the ultimate opening, Proc. of the 9th Intern. Symposium on Mathematical Morphology and Its Application to Signal and Image Processing, ISMM '09, Springer-Verlag, 2009, pp. 272–281.
[31] S. Loncaric, A survey of shape analysis techniques, Pattern Recognit. 31 (1998) 983–1001.
[32] R.C. Veltkamp, M. Hagedoorn, State-of-the-art in shape matching, Tech. rep., Principles of Visual Information Retrieval, 1999.
[33] G. Charpiat, O. Faugeras, R. Keriven, Approximations of shape metrics and application to shape warping and empirical shape statistics, Found. Comput. Math. 5 (1) (2005) 1–58.
[34] R.C. Veltkamp, M. Hagedoorn, Shape similarity measures, properties, and constructions, In Advances in Visual Information Systems, 4th Intern. Conf., VISUAL 2000, Springer, 2000, pp. 467–476.
[35] J. Benner, A. Geiger, K. Leinemann, Flexible generation of semantic 3d buildings models, First Intern. Workshop on Next Generation 3D City Models, 2005.
[36] P. Müller, G. Zeng, P. Wonka, L.V. Gool, Image-based procedural modeling of facades, ACM Trans. Graphics 26 (3) (2007) 85–93.
[37] A. Hanbury, J. Serra, Mathematical morphology in the hls colour space, Proc. of the British Machine Vision Conf. 2001, BMVA, 2001, pp. 451–460.
[38] H. Mayer, S. Reznik, Building facade interpretation from image sequences, CMRT05, Object Extraction for 3D City Models, Road Databases and Traffic Monitoring - Concepts, Algorithms, and Evaluation, Vol. XXXVI, 2005, pp. 55–60.
[39] F. Korč, W. Förstner, eTRIMS Image Database for interpreting images of man-made scenes, Tech. Rep. TR-IGG-P-2009-01, Dept. of Photogrammetry, University of Bonn URL, http://www.ipb.uni-bonn.de/projects/etrims_db/, April 2009.
[40] Z. Yin, X. Zhou, C. Bakal, F. Li, Y. Sun, N. Perrimon, S.T.C. Wong, Using iterative cluster merging with improved gap statistics to perform online phenotype discovery in the context of high-throughput rnai screens, BMC Bioinformatics 9 (2008) 264.
[41] L. Vincent, E.R. Dougherty, Morphological segmentation for textures and particles, in: E.R. Dougherty (Ed.), Digital Image Processing Methods, Marcel Dekker, New York, 1994, pp. 43–102.